Tunable order in alginate/graphene biopolymer nanocomposites

ABSTRACT

We report on highly aligned graphene oxide or graphene sheets inside an alginate matrix and their structure obtained for various compositions. The order of the platelet particles with respect to one another has been verified by environmental scanning microscopy (ESEM) and 2-Dimensional X-ray Diffraction (2D XRD). The microscopic order within the platelet particles has been analyzed by X-ray diffraction (XRD) measurements in the Bragg-Brentano reflection configuration as well as in Debye-Scherrer diffraction mode. The azimuthal angle intensity profiles obtained from 2D XRD analysis have been fit to Maier-Saupe and affine deformation model predictions and the affine deformation model proved to be the most reliable to quantify the order parameter <P2>-values of graphene oxide/sodium alginate and graphene/calcium alginate composites with different weight fractions of the filler. The <P2>-values for graphene oxide/sodium alginate composites were found to show little dependence on the concentration of graphene sheets above ~10 wt%, with a maximum <P2>-value of 0.8 at 25 wt% graphene oxide inside the sodium alginate matrix. The alignment of graphene sheets inside the calcium alginate matrix has been observed to be lower, with an average <P2>-value of 0.7. We have not observed preferred orientation of graphene sheets inside the barium alginate matrix. The formation of a highly aligned graphene oxide/sodium alginate composite structure has been explained by the affine deformation model, whereupon

drying the developed yield stress causes sheets to align in-plane with the polymer matrix. The impaired orientation of graphene sheets inside the calcium alginate matrix and absence of orientation in the barium alginate matrix have been explained by the structure development in the polymer matrix itself due to metal-ion induced cross-linking.

KEYWORDS

Sodium alginate, graphene oxide, composite, order parameter

Introduction

It has been widely reported that inclusion of graphene into polymer matrices yields composite materials with improved mechanical [1], thermal [1b, 2], electrical [3], and gas barrier properties [4]. However, the hydrophobic nature of graphene, its poor dispersibility in many of the commonly used solvents and its consequent propensity to aggregate readily, hampers preparation of graphene-polymer composites with optimal properties. In order to facilitate processability and good dispersion of the sheets, graphene oxide (GO) is often used both as a filler itself or as a precursor of graphene filler [5]. The oxygenated groups on GO sheets enable dispersion in aqueous media, thus making it attractive for the preparation of composites with water-soluble polymers, such as polyvinyl alcohol [6] or chitosan [7]. The addition of GO also yields composite materials with enhanced mechanical [7-8] and gas barrier properties [6, 9].

Recently, several studies [10] reported on the properties of GO-sodium alginate composites. Alginates are naturally occurring copolymers that have been renowned for their gelling properties with multivalent metal ions [11], and have been widely utilized in food industry and for medical applications [12]. Amongst the reported properties of sodium alginate-GO composites, some authors discussed the preferential alignment of GO sheets within the polymer matrix and the unusual changes in morphology upon inclusion of the sheets. However, they did not make an attempt to quantify the degree of orientation of the sheets nor interpret its origin.

In this study, we aim to explore the nature of the alignment of graphene oxide or graphene sheets within an alginate matrix and assess the orientation quantitatively as a function of weight fraction of sheets within the polymer matrix. We also investigate how an alkaline earth metal ion influences

the morphology of alginate and subsequently its composites of various weight fractions of graphene oxide or graphene sheets with regard to their degree of order.

Experimental section

Sodium alginate salt (Protanal® RF 6650) was kindly provided by FMC Biopolymer. To prepare 1 wt% aqueous polymer solution, 1 gram of sodium alginate salt (SA) was dissolved in 99 grams demineralized water, containing 0.4 grams of glycerol (99+ Pure, Acros Organics) under vigorous stirring until a homogenous solution was attained.

Graphene oxide (GO) was prepared via Kovtyiukhova's method [13]. Composite films with various weight fractions of GO were prepared by drop-wise addition of aqueous GO dispersion into a 1 wt% SA solution and continuous stirring until a homogenous mixture was attained. The mixture then was poured into a Petri dish and dried under vacuum at 50 °C overnight (about 15 h).

Subsequently, the thus obtained free-standing water-soluble SA/GO composite films were cut into fine strips of about 30x3 mm^2 and immersed into a 5 wt% $CaCl_2$ (Sigma Aldrich) or a 5 wt% $BaCl_2 \cdot 2H_2O$ (Riedel-de Haën) solution for 20 min to obtain alkali metal cross-linked alginate composite films. The excess salt was removed using copious amounts of demineralized water. The samples were dried under vacuum at 50 °C. Note, that without the cross-linking salt, the SA/GO films readily dissolve in water, they are hydrophilic whereas the cross-linked films are water-insoluble.

Finally, the reduced graphene oxide (rGO)/alginate composite films were prepared by immersing the water-insoluble alkali metal cross-linked alginate/GO composite films, as described above, into an aqueous hydrazine (Sigma Aldrich) solution for 48 h at ambient temperature. The weight ratio of GO to hydrazine was about 10:7. During the course of reduction, the composite films changed their color appreciably, from dark brown to black. After

reduction, the composite films were washed with demineralized water, dried under vacuum at 50 °C and stored in the desiccator with silica gel as the drying agent.

A couple of separate SA/GO mixture samples were disturbed after 3h and 7h of the drying process by stirring them with a spatula for about 30 seconds and subsequently leaving them to dry the rest of the night (about 12 or 8 h).

The cross-sectional images and electron microprobe images of the samples were collected by Environmental Scanning Electron Microscopy (ESEM) using a Philips XL30 Series ESEM. Prior to imaging, the samples were coated with graphite using a Leica EM CED030 sputter coating.

X-ray diffraction (XRD) measurements in Bragg-Brentano reflection mode were performed by a PANalytical X'Pert Pro PW3040/60 diffractometer with Cu Kα radiation operating at 45kV and 40 mA in an angular 2θ range of 5 – 50 ˚.

2-Dimensional X-ray Diffraction (2D XRD) measurements were carried out using a Bruker D8 Discover X-ray diffractometer with a Hi-Star 2D detector and with Cu Kα radiation filtered by cross-coupled Göbel mirrors operated at 40kV and 40mA. The distance between the samples and the detector was maintained at 6 cm and 13 cm for perpendicular and parallel directions to the sample plane, respectively.

Atomic force microscopy (NTMDT Ntegra) (AFM) was used to observe the morphology of graphene oxide sheets. For analysis, 0.05wt% graphene oxide aqueous dispersion was spin-coated on a clean silicon wafer (Siltronix) and examined in tapping mode.

Figure 1a depicts a typical AFM image of the obtained GO sheets. The thickness, measured from the height profile of the AFM image, Figure 1b, shows that the average thickness of the sheets is about 1.0 nm, which indicates the formation of single-layered exfoliated GO [14]. The

lateral dimensions of the sheets vary from sheet to sheet, however, the average length/width ratio – hence aspect ratio – is considered to be high.

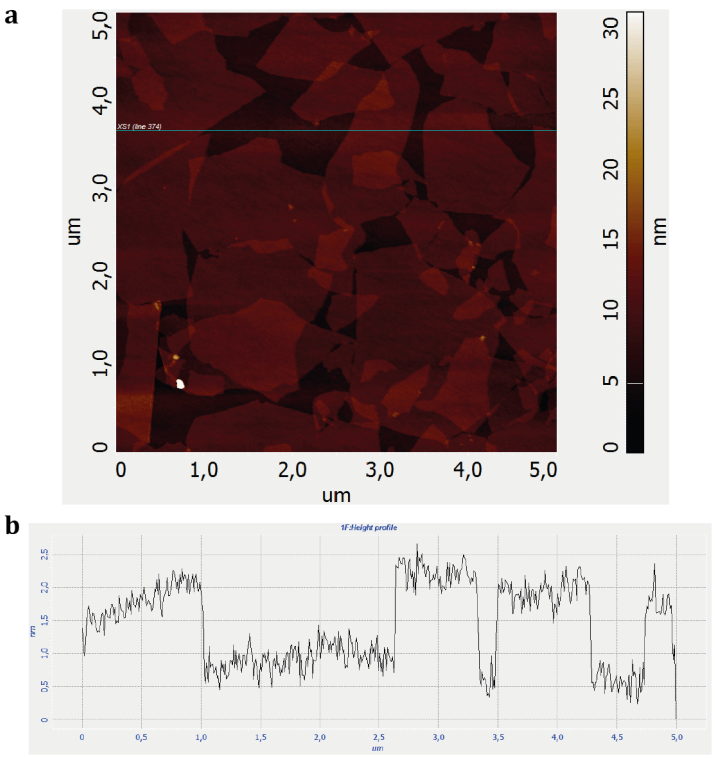

Figure 1. Tapping mode AFM image (a) of graphene oxide sheets on a silica substrate and the height profile (b) corresponding to the line in the AFM image

Results and discussion

Orientation

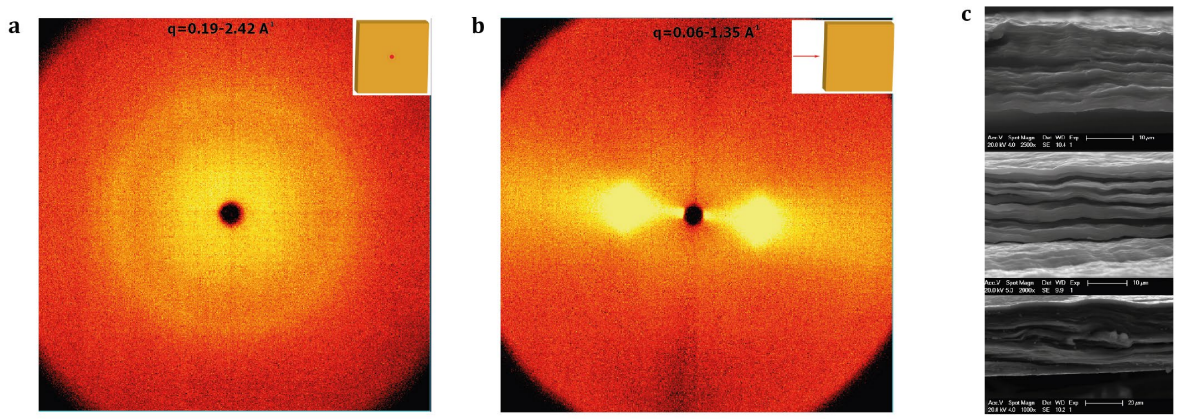

Figure 2. Representative 2D XRD images of sodium alginate/25wt% GO samples with the X-ray beam (inset) along (a) (q=0.19-2.42 $Å^{-1}$) and almost perpendicular (b) (q = 0.06-1.35 $Å^{-1}$) to the layer normal. Graph (c) shows cross-sectional ESEM-images of sodium alginate/25wt% GO (top, scale bar 10 μm) calcium alginate/25wt% Gr (middle, scale bar 10 μm), and barium alginate/25 wt% Gr (bottom, scale bar 20 μm).

Figures 2a and 2b show 2D XRD patterns of the 25 wt% GO/SA composite sample analyzed along (2a) and almost perpendicular (2b) to the layer normal that reveals the ordering of the platelet particles with respect to one another inside the polymer matrix. The diffusive scattering ring around the layer normal reveals isotropic scattering, which originates from the GO sheets that are randomly positioned in the plane of the film. In contrast, the scattering pattern almost perpendicular to the layer normal demonstrates intense equatorial scattering, indicating preferential alignment of the sheets in the polymer matrix. The ESEM micrographs presented in Figure 2c confirm the in-plane orientation of sheets inside a polymer matrix.

Recently, highly ordered alginate/Montmorillonite samples have been obtained by a similar procedure as reported here [15]. These authors have explained the formation of the highly ordered composite by the creation of a network between the negatively charged alginate backbone and the positively charged Montmorillonite edges. Upon drying these samples, a yield stress develops that causes the clay platelets to align. We suggest that the same mechanism is responsible for the alignment of GO sheets although the interactions between the oxygenated GO groups and the polymer backbones are of a different nature. These interactions have been studied recently by Chen et al [10d] who analyzed GO/SA composite paper by means of Fourier Transform Infrared Spectroscopy (FTIR) and X-ray Photoelectron Spectroscopy (XPS). They concluded that the widely abundant hydroxyl groups of the SA chains interact with the carbonyl and/or the epoxy groups as are present on GO sheets by forming hydrogen bonding networks. We will discuss the mechanism of the alignment of GO sheets further in the Discussion section.

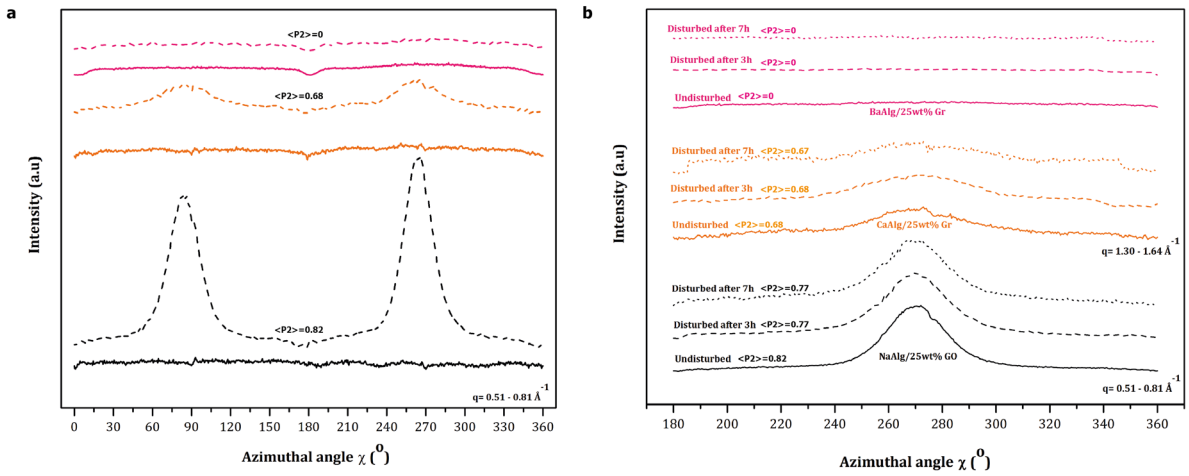

Figure 3. a) Azimuthal angle χ plots for the samples with the X-ray beam parallel to the sample plane: Na Alg (black solid line), Na Alg/25wt% GO (black dashed line), Ca Alg (orange solid line), Ca Alg/25wt% Gr (orange dashed line), Ba Alg (pink solid line), Ba Alg/25wt% Gr (pink dashed line) b) Azimuthal angle χ plots for the samples with the X-ray

beam parallel to the sample plane. The samples have been disturbed at different times during the drying process

Figure 3a illustrates the dependence of the X-ray scattering intensity ($q = 0.51 – 0.81$ Å^{-1}) on azimuthal angle with parallel incidence to the film plane for the samples containing either no GO filler or 25wt% filler. For all the samples we observed isotropic scattering upon incidence perpendicular to the plane as illustrated in Figure 2a indicating no significant alignment, whereas the scattering intensity with incidence parallel to the sample plane varies with the amount of the filler. As can be seen in Figure 3, neither sodium alginate nor calcium or barium alginate polymer chains show preferential in-plane alignment. In contrast, the sodium alginate / 25 wt% GO composite film exhibited two distinct peaks at $\chi = 90°$ and $\chi = 270°$. The scattering intensity of calcium alginate/25 wt% graphene composite sample is similar albeit reduced, and the two distinct peaks are broadened despite the fact that the graphene sheets are aligned in the calcium alginate matrix. The barium alginate/25 wt% graphene composite reveals no significant X-ray scattering dependence on the azimuthal angle.

Figure 3b shows the dependence of the X-ray scattering intensity on azimuthal angle for the samples containing 25 wt% filler and parallel incidence to the film plane that have been disturbed at different times during the drying process. The distinct peak at $\chi = 270°$ remains present for sodium alginate/25 wt% GO composite and calcium alginate/25 wt% graphene composite samples indicating no apparent disorder of the filler sheets upon disturbance. As before, the barium alginate/25 wt% graphene reveals no significant X-ray scattering dependence on the azimuthal angle both for the disturbed and undisturbed systems.

Microscopic structure

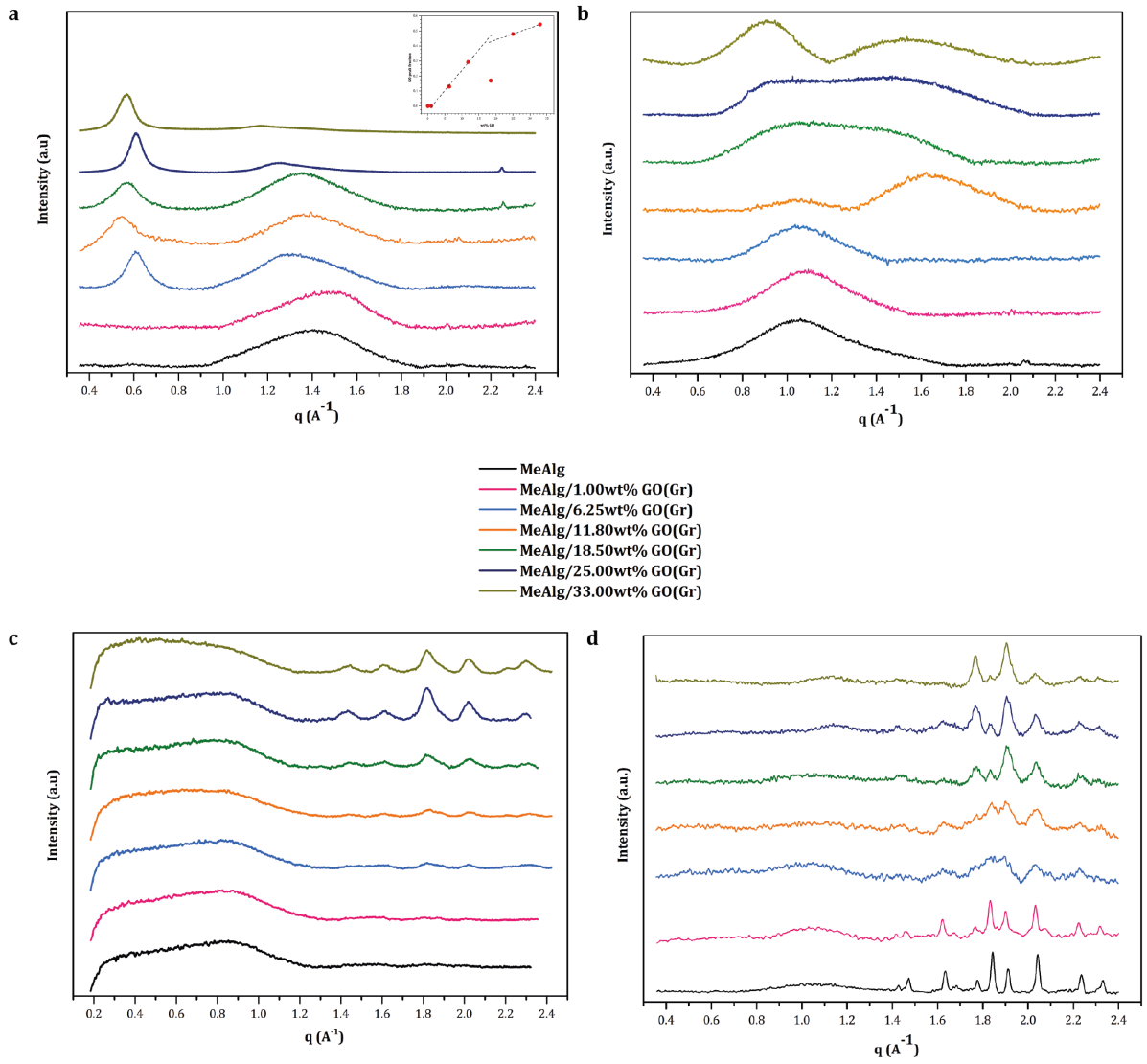

Figure 4. a) X-ray scattering patterns of Na Alg/ GO composite films collected in the Bragg-Brentano reflection configuration. The inset spectrum represents relative fractional scattering from GO versus the concentration of GO. b) X-ray scattering patterns of Ca Alg/ Gr composite films collected in the Bragg-Brentano reflection configuration. c) X-ray scattering patterns of Ba Alg/ Gr composite films with the beam along to the layer normal collected in

in Debye-Scherrer diffraction mode. d) X-ray scattering patterns of Ba Alg/ Gr composite films collected in the Bragg-Brentano reflection configuration

The microscopic order of the samples of various compositions has been analyzed by XRD in the Bragg-Brentano reflection configuration and is presented in the Figure 4a-d. The Figure 4c represents the microscopic order of the samples of various compositions collected in Debye-Scherrer diffraction mode (done on the 2D XRD instrument). As shown in Figure 4a, with increasing concentration of GO, the peak at ~0.6 $Å^{-1,}$, corresponding to an interlayer spacing of ~11 Å between GO sheets, becomes more prominent. Using the Scherrer equation [16], the apparent width of an ordered stack of graphene oxide sheets was found to be ~144 Å, which yields to 13-14 sheets per stack. The absence of this peak at low weight fractions of filler indicates complete exfoliation of GO sheets [17]. In actual fact the intensities are never very high which indicates a relatively low degree of stacking. The broad peak at ~1.4 $Å^{-1}$ corresponds to an amorphous structure of sodium alginate with an average intermolecular distance between the polymer chains of 4.5 Å. This value is ~ 2 Å smaller than the value reported previously[10a, 10c]. We attribute the reduced interlayer spacing between the polymer chains to the drying process at an elevated temperature and under vacuum that enables to achieve almost water-free polymer film samples. With an increasing amount of GO, the distance between the neighboring chains increases to ~5.2 Å, which we attribute to the intercalation of the sheets between the polymer chains. The inset graph shows the relative fractional scattering from GO versus the content of GO. As the amount of GO in the polymer matrix increases, the relative scattering fraction from GO sheets becomes larger due the growing number of scattering centers. We have observed the initial slope of ~2, which corresponds well to C/O ratio in GO, which is often reported to be 4:1 – 2:1. [18] At high GO concentrations, the relative scattering fraction from GO becomes less concentration dependent presumably due to the onset of stacking of GO sheets and multiple scattering effects.

Figure 4b represents the XRD patterns obtained in reflection mode for calcium alginate and its graphene composite films. Upon cross-linking alginate chains with calcium ions, the average distance between the polymer chains increased up to 6.3 Å, a similar value as has been reported previously [19]. With increasing amount of graphene, a new peak evolves at ~1.7 $Å^{-1}$, corresponding to an interlayer distance between graphene sheets of ~3.7 Å. As the concentration of graphene increases, two distinctive peaks merge and separate again at 33 wt% of filler. The original polymer peak shifts towards higher inter-spacing values with increasing amount of graphene, which suggests that the intercalated structure remains intact during the ion exchange reaction and subsequent reduction of the GO sheets. A small increment in the distance (up to ~4 Å) between graphene sheets can be also observed with an increased concentration of the filler.

Figure 4c shows spectra of barium alginate and its graphene composites of various compositions spectrum measured with 2D XRD perpendicular to the plane of the samples. Here, with an increasing concentration of graphene, the peak at 1.8 $Å^{-1}$ becomes distinctively higher, and is accompanied by another set of four growing peaks at 1.4 $Å^{-1}$, 1.6 $Å^{-1}$, 2.0 $Å^{-1}$ and 2.2 $Å^{-1}$ albeit the latter less intense. This suggests that with increasing amount of graphene, an incommensurate modulated structure is formed [20], which seems to impair the alignment of the sheets as shown in Figure 3a. The system develops a central peak 1.8 $Å^{-1}$ and the satellite peaks at the above mentioned positions, corresponding to repeat distances of ~16 Å , a distance that is well compatible with the average domain size of 126 Å as obtained from the width of the 1.8 $Å^{-1}$ peak using the Scherrer formula. The peak at 2.3 $Å^{-1}$ is ascribed to the in-plane (104) graphite reflection [21]. The X-ray scattering in reflection mode presented in Figure 4d reveals more details. Surprisingly, we could observe the semi-crystalline structure of the barium alginate sample, containing nearly 30 wt% of glycerol. The spectrum also revealed additional peaks, which have not been observed in the 2D XRD experiment. The data collected

in reflection mode corroborate the observations discussed earlier, however with some deviations. A new peak at ~1.9 $Å^{-1}$ becomes apparent, and the two peaks at 1.4 $Å^{-1}$ and 1.6 $Å^{-1}$ vanish for the Ba Alg/33 wt% Gr sample. Nonetheless, the peaks at 2.0 $Å^{-1}$ and 2.2 $Å^{-1}$ remain at their position, thus not entirely dismissing our assessment of the development of the incommensurately modulated structure.

Interpretation of data collected in transmission mode, Figure 4c, is somewhat involved. First of all, the information of the sample structure is almost entirely lost at the initial part of the spectrum due to the broadening of the polymer peak. Secondly, the inconsistency between data collected in transmission mode and reflection mode can be further explained by fundamental differences between the two measurement techniques and dissimilar scattering vector directions (see Supporting Information Figure S1). First of all, due to the small film thickness compared to the penetration depth of the beam, both techniques should probe the total film. However, the path length of the incident and diffracted beam in transmission mode through polymer material is on average longer than in reflection mode which will be responsible for the blurring of the signal obtained in transmission mode. The diffracted beam in the reflection mode is moreover refocused at the detector slits which significantly improves the resolution. In addition, the scattering vector remains parallel to the normal for reflection mode and varies orientation for the transmission mode. This implies, that the form factor of the scattering centers varies differently for the two techniques which might explain dissimilar intensity variations of peaks with diffraction angle.

Order parameter

It is well established that the azimuthal angle profile can be used to quantify the orientational order parameter $\langle P_2 \rangle$ [22]. For perfectly aligned samples $\langle P_2 \rangle = 1$, whereas for randomly oriented samples $\langle P_2 \rangle = 0$. The degree of orientation can be calculated using Maier-Saupe [23] or affine deformation [24] models for the structure of the composite. The former model is formulated on the basis of long-ranged anisotropic interactions between molecules inducing orientation in one particular direction. The latter one assumes a uniform reduction of intermolecular spacing upon overall deformation. As discussed earlier, we surmise that the drying step induces orientation of the sheets, so the affine deformation model is expected to be the more valid. In order to verify this presumption and compute $\langle P_2 \rangle$, we first fit our data by two distribution functions to examine, which of these yields the best fit. In the first attempt, data from intensity profiles of an azimuthal angle were fit by an intensity profile involving the Maier-Saupe (MS) distribution function [22a]

$$I(\chi) = I_b + Ae^{\alpha \cos^2(\chi)} \qquad (1)$$

where I_b is the baseline intensity, A a constant representing the relative scattering intensity, α the width of the distribution and χ the azimuthal angle.

The same data were also fit to an intensity profile involving the affine deformation (AD) distribution function:

$$I(\chi) = I_b + A\frac{\cos^3\left[\tan^{-1}\left(\lambda \tan(\chi)\right)\right]}{\cos^3(\chi)} \qquad (2)$$

where I_b , A and χ as previously mentioned, and λ the degree of vertical compression as described in [15].

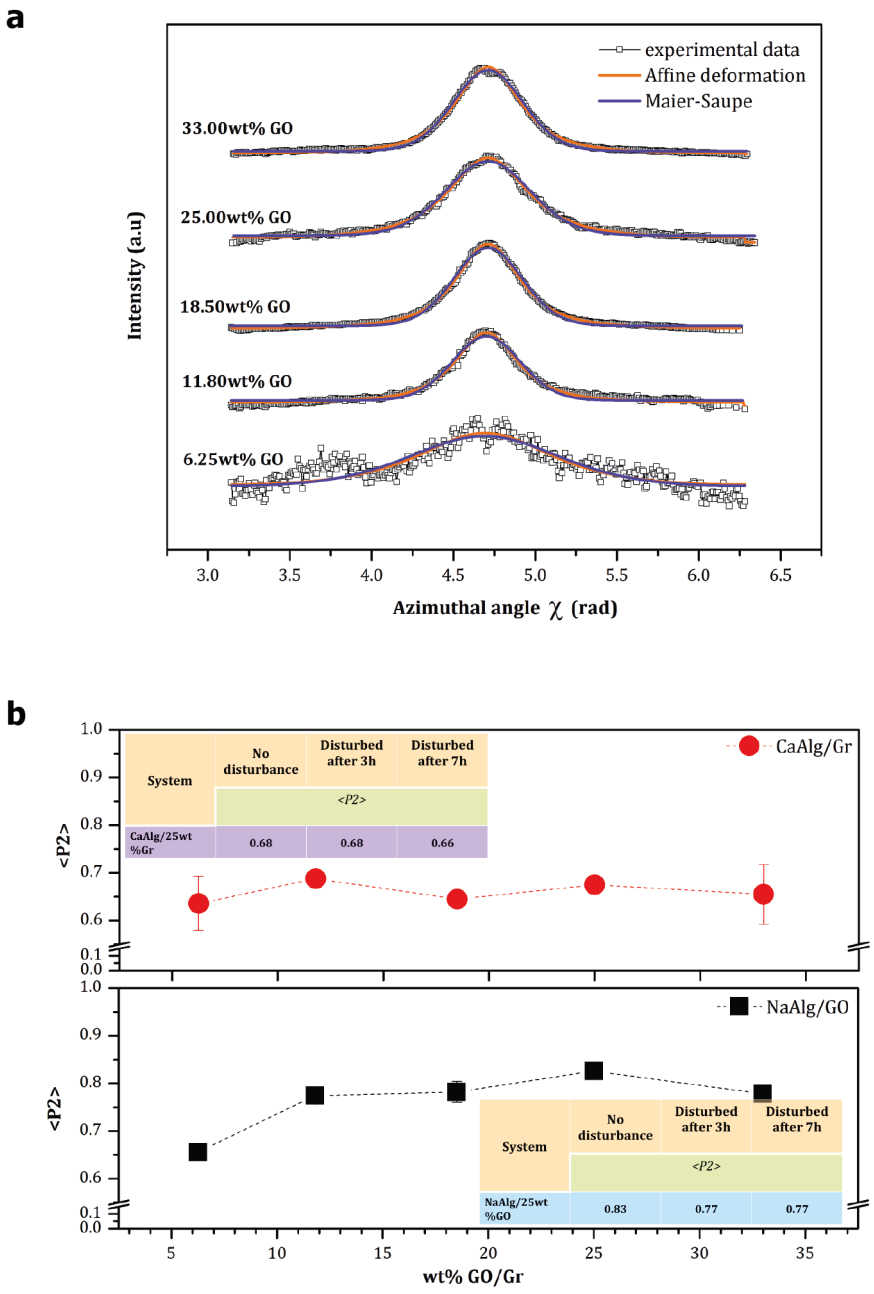

Figure 5. a) Azimuthal angle χ profile of the scattering intensity. The solid lines represent affine deformation (orange) and Maier-Saupe (violet) distribution function fits. b) Order parameter $<P_2>$ dependence on GO/Gr concentration. The inset shows the order parameter values of the systems that have been disturbed at various times during the drying process

From Figure 5a we see that both orientation distribution functions provide good fits, albeit that the affine deformation function describes the data points slightly better, especially near the tails. Hence, the AD model was used to quantify $\langle P_2 \rangle$ although the values obtained for the MS model were very similar.

From the fit values of the vertical degree of compression (λ), the order parameter $\langle P_2 \rangle$ was determined using

$$\langle P_2 \rangle = \frac{\int_{-1}^{1} P_2(\cos\chi) F(\chi) d\cos\chi}{\int_{-1}^{1} F(\chi) d\cos\chi} \quad (3)$$

with the second-order Legendre polynomial

$$P_2(\cos\chi) = \frac{1}{2}\left(3\cos^2\chi - 1\right) \quad (4)$$

and where F(χ) is the Affine Deformation distribution function in eq.(2). The calculated $\langle P_2 \rangle$ values are presented in the Figure 5b. Remarkably, high order parameter values are achieved for the SA/GO composites, which compare favorably to values reported for GO sheets aligned under magnetic field [25]. With higher amounts of GO, the order parameter values tend to decrease presumably due to jamming effects of neighboring GO sheets. The degree of alignment of graphene sheets in calcium alginate is inferior and appears to be less dependent of the weight fraction of the filler.

Discussion

Table 1. Characteristic properties of different alginate composites

System	Factor			
	Sheet order parameter	*Structure*	*Concentration effects*	
			<P2>	*Structure*
NaAlg/GO	**Highest**	**Amorphous**	**Varies little > 10wt%**	**No**
CaAlg/Gr	**Moderate**	**Amorphous**	**Slightly decreases >10wt%**	**No**
BaAlg/Gr	**Non-existing**	**Semi-crystalline**	**-**	**Varying**

As presented in the Table 1, it is apparent that different types of alginate composites exhibit dissimilar properties. Though both sodium alginate/graphene oxide and calcium alginate/graphene systems possess an amorphous structure even with increasing amount of filler, the order parameter values differ significantly. We emphasize, that the first drying step is the important step to obtain highly ordered sodium alginate/graphene oxide composites. As mentioned earlier, the interactions between carbonyl and epoxy groups present on the GO sheets and hydroxyl groups on the sodium alginate polymer chains involve the formation of a hydrogen bonding network. Before drying, the mixture of sodium alginate and graphene oxide is isotropic as orientational freedom of graphene oxide sheets is not severely restricted. Upon drying, the strength of the hydrogen-bonding network between the two species increases, the mixture begins to gel and the viscosity of the mixture increases upon evaporation of water. As the drying continues, stress begins to develop in the system causing graphene oxide sheets to align in-plane. At a critical value, the critical gelation point, the system forms a rigid gel,

whereupon graphene oxide sheets remain permanently locked inside the polymer matrix. The gelled polymer matrix subsequently shrinks further upon drying leading to the observed high level of alignment. The results, presented in Figure 3b, indicate a significant degree of resilience of sodium alginate/25 wt% graphene oxide system to disturbance while drying. As described in the experimental procedure, a couple of separate mixture samples were disturbed after 3 hours and 7 hours during the drying process. The <P2> values of the perturbed sodium alginate/25 wt% graphene oxide system varied a little but overall the <P2> values remained quite high (<P2> = 0.77). This indicates that below the critical gelation point, the developing stress is able to reinstate the alignment of graphene oxide sheets and suggests that the transition point is rather abrupt. The <P2> values of the perturbed calcium alginate/25 wt% graphene system showed little change, if any change at all. The perturbed barium alginate/25wt% graphene system revealed no changes in <P2> values. The influence of an alkali earth metal cation and the reduction reaction medium are discussed in the next paragraph.

The experimental data shows (Figure 5) that the order parameter values are not significantly affected by increasing graphene oxide concentration above ~10 wt%. However, beyond ~30 wt%, the order parameter value slightly decreases. We suggest that at higher weight fractions of graphene oxide, the level of exfoliation of graphene oxide sheets decreases as the sheets begin to stack. As a result of drying, the system begins to gel at a higher solids concentration, which, in turn, adversely affects ordering of the sheets.

In addition, the alignment of the sheets is also influenced by the presence of alkaline earth metal cations, in particular by their size as well as their affinity to the polymer matrix and the GO sheets. It is well known that some metal cations exhibit different affinity to the alginate matrix, such as that barium ions have higher binding affinity to alginate than calcium ions [11]. Furthermore, a recent study [26] has shown that Ca^{2+} and Ba^{2+} cations intercalate in between GO

sheets and strongly interact with sp^2 clusters of GO sheets through cation - π interactions. The study also has shown that the metal ions can bind to different positions of the graphene sheets, and that the binding energy not only depends on the position, but also on the metal cation. These results indicate that the barium ion binds stronger than calcium to graphene sheets. A preceding investigation [27] into competitive binding between alkaline earth metal ions with water and benzene has concluded that the solvent exchange rate between the cations and benzene strongly depends on the solvation extent of a cation. The study shows that barium rapidly exchanges water molecules with benzene, whereas the rate of exchange for calcium strongly depends on the extent of solvation, showing the tendency to decrease with increasing level of hydration. On the basis of the above information, we suggest that during the reduction reaction of GO in aqueous hydrazine medium, competing reactions between oxygenated groups on the alginate backbone, sp^2 clusters of rGO sheets, water molecules and alkaline earth metal ions take place, thus strongly affecting the orientation of the sheets inside the polymer matrix.

Surprisingly, we have found that barium alginate, containing nearly 30 wt% of glycerol, possesses a semi-crystalline structure. To exclude the possibility of recrystallization of the barium chloride salt and potential contamination, we performed XRD and elemental mapping experiments and found that corresponding scattering peaks of the salt do not at all match with the scattering pattern obtained for barium alginate system nor did we find any traces of contamination (see Supporting Information Figure S2 and Figure S3). With increasing amount of graphene, the original semi-crystalline structure of barium alginate is not destructed, but rather modified by the presence of the sheets resulting in what appears to be an incommensurate modulated structure. We speculate that structural changes begin taking place during the cross-linking procedure, and the system once again reorganizes itself during the reduction reaction in a complicated manner as discussed before.

Conclusions

We conclude, that highly aligned graphene oxide (or graphene) sheets in an alginate matrix can be obtained by a simple preparation method without the need of an external field. This was verified by various techniques. ESEM micrographs have allowed us to observe a highly dense and layered structure of the composite samples of various compositions. XRD studies have shown that different morphological structures can be formed upon cross-linking alginate with the divalent alkali metal ions in the presence of the filler. The preferential alignment of the sheets has been confirmed by 2D XRD experiments. The affine deformation model can accurately describe the data and confirms the formation of highly ordered structures due to gelling and the associated yield stress development upon drying the samples.

The degree of alignment is influenced by several factors. Our study has shown, that competing interactions between an alkali metal ion, graphene oxide sheets and the polymer matrix in the aqueous environment render a range of possible order parameter values. Furthermore, the degree of order in the sodium alginate matrix shows strong graphene oxide concentration dependence. Nevertheless, it is clear that our composite systems could be employed as potential gas barrier coatings comparable to what has been attained by other workers in the field [28] as the present results show that it is possible to make highly aligned composite films without requiring any complicated or time consuming preparation methods, such as layer-by-layer deposition.

ACKNOWLEDGMENTS

This work is supported by NanoNextNL, a micro and nanotechnology consortium of the Government of the Netherlands and 130 partners. The authors appreciate Arjan Thijssen's help collecting ESEM images, and acknowledge fruitful discussions with J. Zlopasa.

SUPPORTING INFORMATION

Schematic illustration of the scattering vector in transmission and reflection modes in the X-ray diffraction measurement is presented in the **Figure S1.**

X-ray scattering patterns of $BaCl_2$ x $2H_2O$ (black solid line) and Ba Alg (red solid line) sample film collected in reflection mode are presented in the **Figure S2**.

Electron microprobe images obtained of barium alginate/25wt% graphene sample are presented in the **Figure S3**.

This material is available free of charge via the Internet at http://pubs.acs.org.

REFERENCES

1. (a) Zhao, X.; Zhang, Q. H.; Chen, D. J.; Lu, P. *Macromolecules* **2010,** *43* (5), 2357-2363; (b) Song, P. G.; Cao, Z. H.; Cai, Y. Z.; Zhao, L. P.; Fang, Z. P.; Fu, S. Y. *Polymer* **2011,** *52* (18), 4001-4010.

2. Wang, X.; Yang, H. Y.; Song, L.; Hu, Y.; Xing, W. Y.; Lu, H. D. *Compos Sci Technol* **2011,** *72* (1), 1-6.

3. (a) Qi, X. Y.; Yan, D.; Jiang, Z. G.; Cao, Y. K.; Yu, Z. Z.; Yavari, F.; Koratkar, N. *Acs Appl Mater Inter* **2011,** *3* (8), 3130-3133; (b) Liao, K. H.; Qian, Y. Q.; Macosko, C. W. *Polymer* **2012,** *53* (17), 3756-3761.

4. (a) Kim, H.; Miura, Y.; Macosko, C. W. *Chem Mater* **2010,** *22* (11), 3441-3450; (b) Kuila, T.; Bose, S.; Mishra, A. K.; Khanra, P.; Kim, N. H.; Lee, J. H. *Polym Test* **2012,** *31* (1), 31-38.

5. Kuila, T.; Bose, S.; Mishra, A. K.; Khanra, P.; Kim, N. H.; Lee, J. H. *Prog Mater Sci* **2012,** *57* (7), 1061-1105.

6. Kim, H. M.; Lee, J. K.; Lee, H. S. *Thin Solid Films* **2011,** *519* (22), 7766-7771.

7. Yang, X. M.; Tu, Y. F.; Li, L. A.; Shang, S. M.; Tao, X. M. *Acs Appl Mater Inter* **2010,** *2* (6), 1707-1713.

8. Xu, Y. X.; Hong, W. J.; Bai, H.; Li, C.; Shi, G. Q. *Carbon* **2009,** *47* (15), 3538-3543.

9. Kang, H. L.; Zuo, K. H.; Wang, Z.; Zhang, L. Q.; Liu, L.; Guo, B. C. *Compos Sci Technol* **2014,** *92*, 1-8.

10. (a) Ionita, M.; Pandele, M. A.; Iovu, H. *Carbohyd Polym* **2013,** *94* (1), 339-344; (b) Cao, K. T.; Jiang, Z. Y.; Zhao, J.; Zhao, C. H.; Gao, C. Y.; Pan, F. S.; Wang, B. Y.; Cao, X. Z.; Yang, J. *J Membrane Sci* **2014,** *469*, 272-283; (c) Valentini, L.; Rescignano, N.; Puglia, D.; Cardinali, M.; Kenny, J. *Eur J Inorg Chem* **2015,** (7), 1192-1197; (d) Chen, K.; Shi, B.; Yue, Y.; Qi, J.; Guo, L. *Acs Nano* **2015,** *9* (8), 8165–8175.

11. Haug, A.; Smidsrod, O. *Acta Chem Scand* **1970,** *24* (3), 843-854.

12. Pawar, S. N.; Edgar, K. J. *Biomaterials* **2012,** *33* (11), 3279-3305.

13. Kovtyukhova, N. I.; Ollivier, P. J.; Martin, B. R.; Mallouk, T. E.; Chizhik, S. A.; Buzaneva, E. V.; Gorchinskiy, A. D. *Chem Mater* **1999,** *11* (3), 771-778.

14. (a) Stankovich, S.; Piner, R. D.; Chen, X. Q.; Wu, N. Q.; Nguyen, S. T.; Ruoff, R. S. *J Mater Chem* **2006,** *16* (2), 155-158; (b) Kulkarni, D. D.; Choi, I.; Singamaneni, S.; Tsukruk, V. V. *Acs Nano* **2010,** *4* (8), 4667-4676.

15. Zlopasa, J.; Norder, B.; Koenders, E. A. B.; Picken, S. J. *Macromolecules* **2015,** *48* (4), 1204-1209.

16. Scherrer, P. *Göttinger Nachrichten Math. Phys* **1918**, 98-100.

17. Kim, H.; Abdala, A. A.; Macosko, C. W. *Macromolecules* **2010,** *43* (16), 6515-6530.

18. Pei, S. F.; Cheng, H. M. *Carbon* **2012,** *50* (9), 3210-3228.

19. (a) Li, L. B.; Fang, Y. P.; Vreeker, R.; Appelqvist, I. *Biomacromolecules* **2007,** *8* (2), 464-468; (b) Sikorski, P.; Mo, F.; Skjak-Braek, G.; Stokke, B. T. *Biomacromolecules* **2007,** *8* (7), 2098-2103.

20. van Smaalen, S. *Crystallography Reviews* **1995,** *4* (2), 79-202.

21. Howe, J. Y.; Rawn, C. J.; Jones, L. E.; Ow, H. *Powder Diffr* **2003,** *18* (2), 150-154.

22. (a) Feng, S.; Xiong, X. Q.; Zhang, G. L.; Xia, N.; Chen, Y. M.; Wang, W. *Macromolecules* **2009,** *42* (1), 281-287; (b) Picken, S. J. *Macromolecules* **1990,** *23* (2), 464-470; (c) Picken, S. J.; Aerts, J.; Visser, R.; Northolt, M. G. *Macromolecules* **1990,** *23* (16), 3849-3854.

23. Saupe, A.; Maier, W. *Z Naturforsch Pt A* **1961,** *16* (8), 816-824.

24. Treloar, L. R. G., *The Physics of Rubber Elasticity*. 3rd ed.; Oxford Classic Texts in the Physical Sciences: 2005; p 62.

25. Wu, L. L.; Ohtani, M.; Takata, M.; Saeki, A.; Seki, S.; Ishida, Y.; Aida, T. *Acs Nano* **2014,** *8* (5), 4640-4649.

26. Sun, P. Z.; Zheng, F.; Zhu, M.; Song, Z. G.; Wang, K. L.; Zhong, M. L.; Wu, D. H.; Little, R. B.; Xu, Z. P.; Zhu, H. W. *Acs Nano* **2014,** *8* (1), 850-859.

27. Rodriguez-Cruz, S. E.; Williams, E. R. *J Am Soc Mass Spectr* **2001,** *12* (3), 250-257.

28. (a) Gokhale, A. A.; Lu, J.; Parker, N. J.; Izbicki, A. P.; Sanyal, O.; Lee, I. *J Colloid Interf Sci* **2013,** *409*, 219-226; (b) Yang, Y. H.; Bolling, L.; Priolo, M. A.; Grunlan, J. C. *Adv Mater* **2013,** *25* (4), 503-508; (c) Huang, H. D.; Ren, P. G.; Chen, J.; Zhang, W. Q.; Ji, X.; Li, Z. M. *J Membrane Sci* **2012,** *409*, 156-163.